REVISION 2, Correction date: 01aug 2023

Multi-wavelength Raman spectroscopy of natural nanostructured carbons

Sergey Isaenko[1,*], Tatyana Shumilova[1], Vladimir Bocharov[2], and Vasily Ulyashev[1]

[1]Institute of Geology, Federal Research Centre, Komi Science Centre of the Ural Branch of the Russian Academy of Sciences, Pervomayskaya 54, Syktyvkar 167982, Russia

[2]St. Petersburg State University, Ulyanovskaya 1, St. Petersburg, Peterhof, 198504, Russia

ABSTRACT

There is an extensive range of carbon substances with poorly ordered structures that are not well understood. Yet they are important as indicators of conditions of related geological processes. The carbon minerals include nanocrystalline graphite, natural analogues of glass-like carbon (GLC) – shungite and impact ultrahigh-pressure GLC, recently discovered ultranocrystalline diamond, as well as natural carbon nanocomposites of diamond, lonsdaleite and graphite. Studying these natural carbon substances using a standard Raman approach with excitation by visible radiation may lead to a significant distortion of the understanding of their phase states. This paper presents in detail for the first time the spectral features of natural, poorly ordered and multiphase sp^2-sp^3 carbon composites by multi–wave Raman spectroscopy using laser excitations from visible to ultraviolet light applied to natural low-ordered carbon substances - nanocrystalline graphite and shungite, nanocrystalline and ultranocrystalline diamond, and multiphase carbon aggregates. The carbon state resolution advantages of ultraviolet Raman spectroscopy for phase analysis of nanostructured and poorly ordered polycomponent carbon

This is the peer-reviewed, final accepted version for American Mineralogist, published by the Mineralogical Society of America.
The published version is subject to change. Cite as Authors (Year) Title. American Mineralogist, in press.
DOI: https://doi.org/10.2138/am-2022-8912. http://www.minsocam.org/

substances containing sp^2- and sp^3-carbons are presented. Raman spectroscopy with ultraviolet excitation can also be applied in the analysis of industrial carbon materials, such as glassy carbon and functional carbon nanocomposites, including ultranocrystalline diamond, lonsdaleite, and amorphous sp^3-carbon components.

Keywords: Raman spectroscopy, visible and ultraviolet excitation, natural nanostructured carbons

Introduction

Raman spectroscopy is currently highly sought after as a tool for studying carbon-based substances. Raman spectroscopy can readily identify crystalline substances such as diamond (Krishnan 1946; Ferrari 2002), graphite (Tan et al. 1999a; Tan et al. 2004; Saito 2010; Ferrari 2007; Tuinstra, Koenig 1970), and fullerite (Buseck et al. 1992; Kovalevski 2008). Great opportunities are also open to study molecular (Shumilova et al. 2014, Tan et al. 1999b; Wang et al 2012), amorphous (Golubev et al 2019) and low-ordered carbon substances including soot (Sadezky et al. 2005), shungite (Isaenko et al., 2018; Golubev et al 2016), glassy carbon (Yasumaru et al. 2004), nanocrystalline graphite (Ferrari 2007; Gupta et al. 2003; Khanchuk et al. 2013; Plyusnina et al. 2013; Berdnikov et al 2014; Piscanec et al. 2004), diamond-like carbon (Ferrari 2002, Ferrari, Robertson 2001, 2004; Shumilova et al. 2013), nanocrystalline diamond (Chen et al. 2018; Davydov et al. 2004; Davydov et al. 2006; Goryainov et al 2014; Filik et al. 2006; Prawer et al. 2000; Kis et al., 2016; Shumilova et al. 2016; Mermoux 2017) and ultrananocrystalline diamond (Shenderova 2006; Shumilova et al. 2020). The analysis and interpretation of low-ordered substances are more complex, often necessitating the use of complementary techniques such as transmission electron microscopy (TEM) for structural and chemical analyses. Although amorphous carbon, nanocrystalline diamonds, and diamond-like carbon were studied by multi-wavelength Raman spectroscopy (Ferrari, Robertson 2001, 2004;

Filik et al. 2006), low-ordered/nanocrystalline carbonaceous matters with sp^2 hybridization have mostly been investigated by visible Raman spectroscopy (Wopenka, Pasteris, 1993; Tuinstra, Koenig, 1970; Beyssac et al 2002).

When comparing Raman spectroscopy data of nanocrystalline diamonds, diamond-like carbon, and graphite-like substances, it has been observed that the Raman signal originating from the sp^3 carbon state, which is excited by visible lasers in low-crystalline and amorphous substances, can be overlapped by the D-band of graphite-like carbon (Ferrari, Robertson 2004). It is known that a visible 633 nm laser beam excites a D-band centered at 1330 cm^{-1}, which is a characteristic of low-ordered sp^2 carbon substances, such as shungite (Golubev 2013; Golubev et al. 2016; Sychov et al. 2016) and nanocrystalline graphite (Danilova et al. 2015; Tan 2004; Merlen et al. 2017). The band is close to the diamond T_{2g} mode position at 1332 cm^{-1} (Krishnan 1946), which complicates the interpretation of the Raman spectra of poor-crystalline carbon substances with multiple phases, including nanocrystalline matter, due to the 50–250 times more intense scattering by sp^2 carbon compared to sp^3 sites (Ferrari, Robertson 2004). The latter results in very weak sp^3-carbon band in the spectra of poorly ordered carbon multiphase substances or even complete overlapping by D-band of sp^2-carbon component. For this reason, the sp^3-carbon band becomes invisible and may be neglected in the spectroscopic data interpretation of poorly ordered carbons. In addition, the circumstance may result in misinterpretation of the Raman spectra of diamond or amorphous tetrahedral diamond-like carbon (ta-C) instead of the D-band of sp^2 carbon.

The correct phase diagnostics of carbon substance is largely determined by an accurate interpretation of Raman spectrum bands around 1330 cm^{-1}, which is complicated by different effects of the Raman shift of the D-band of graphite-type substances (Ferrari, Robertson 2001, 2004). In the case of carbon multicomponent materials, it has been observed that the relative

intensities of certain Raman peaks can strongly depend on the wavelength of the laser used for excitation (Ferrari, Robertson 2001, 2004, Mermoux 2017). Thus, the effect could be used in the application of ultraviolet (UV) Raman spectroscopy to solve the problem of Raman bands of sp^2 and sp^3 carbons overlapping in spectra range of near 1330 cm^{-1} (Ferrari, Robertson 2001, 2004, Mermoux 2017). Indeed, UV Raman spectroscopy with excitation wavelengths (λ) ranging from 244 to 364 nm holds promise for the analysis of low-crystalline carbon substances.

UV Raman spectroscopy does not fundamentally differ from routine analysis using visible laser excitation. It has technical advantages that include the absence of fluorescence in the Raman active spectral range and the increase in sensitivity, which is proportional to $1/\lambda^4$ (λ is the laser wavelength). However, due to the higher energy influence of ultraviolet radiation, carbon samples can experience more intense heating, which may result in structural alterations and even combustion in an air atmosphere (Mermoux, 2017), that requires accurate control of energy treatment. In addition, there are specific technical challenges associated with focusing invisible radiation in the optical system and on a sample, where the laser spot is increased to 5 μm^2. This decrease in locality of the analysis leads to a larger area being probed during the measurement. Finally, it is worth noting that the instruments for UV Raman spectroscopy are significantly more expensive and more challenging to operate compared to those used for visible spectroscopy.

Ferrari and Robertson applied multiwavelength Raman spectroscopy in the analysis of low-ordered carbon substances, including amorphous carbon, nanocrystalline diamonds, and diamond-like carbon (Ferrari 2002, 2007; Ferrari, Robertson 2001, 2004). They demonstrated that the presence of a D-band in the Raman spectrum of disordered or amorphous carbons was influenced not only by the quantity of carbon in sp^2-hybridization but also by the nature of its structure. They also showed that with UV laser excitation, D-band was absent in the spectra of

94 crystalline graphites, but the residual D-band could be present in the UV Raman spectrum being
95 shifted to 1400 cm^{-1} only if sp^2 carbon atoms were grouped to disordered rings, and in low-
96 crystalline polymerized substances (Ferrari, Robertson 2001).

97 Moreover, it has been recently discovered (Osipov et al. 2018) that increasing the
98 excitation energy makes sp^3 and sp^2 states more distinguishable. Thus, under UV excitation, sp^2
99 and sp^3 carbon sites become more recognizable.

100 Despite detailed studies of different carbon materials, the spectroscopic characteristics of
101 low-ordered graphite-like substances (sp^2–carbon), including nanocrystalline graphite and
102 shungite, have not been previously examined in detail using UV excitation. In addition, the
103 studies on mixtures of sp^2 and sp^3 carbons are limited.

104 In this paper, we present the results of our systematic studies of low-ordered natural carbon
105 materials by UV Raman spectroscopy including sp^3, sp^2 carbons and their mixtures. Here we
106 present the detailed analysis of UV Raman spectra of ultrananocrystalline diamond,
107 nanocrystalline diamond, polyphase carbon aggregate, nanocrystalline graphite and shungite. The
108 obtained spectroscopic characteristics demonstrate specific structure features and the perspectives
109 for studying low-crystalline multiphase substances with sp^2 and sp^3 carbon states that are
110 important for the identification of sp^3 carbon in either natural specimens or synthesized materials.
111 In particular, we have employed UV Raman spectroscopy to successfully analyze the natural
112 aggregates of ultrananocrystalline diamond with nondiamond carbon on surfaces of diamond
113 nanocrystallites.

114

115 **Samples and experimental methods**

116 In our previous studies, we provided Raman analysis with visible and UV laser excitations
117 of natural samples of poor-ordered sp^2 and sp^3 carbons with known phase states by preliminary

analysis of their chemical composition and structure. Here we present the multiwave Raman data of natural samples from different objects (Fig. 1) – shungite (Shunga, Russia) (Golubev et al. 2016; Melezhik et al 2004; Buseck et al. 1992, 1997 and others), nanocrystalline graphite from graphitic shists of the Nerkayu metamorphic complex in the Subpolar Urals (Russia) (Shumilova et al. 2016); natural ultrahigh-pressure (UHP) glass-like carbon (GLC), natural impact nanocrystalline diamond, ultrananocrystalline diamond and polyphase carbon aggregate from impactites of the Kara giant crater (Pay-Khoy, Russia). The carbons have been described in detail in our papers (Shumilova et al. 2014, 2018a, 2019, Ulyashev et al. 2018).

The visible Raman spectroscopy studies were conducted using LabRam HR800 (Horiba, Jobin Yvon) high-resolution Raman spectrometer at the Center of Collective Use «Geoscience», the Institute of Geology, Federal Research Center of Komi Science Center of Ural Branch of Russian Academy of Sciences, Syktyvkar. Registration conditions: gratings – 1800 and 600 g/mm; confocal hole size – 300 and 500 μm; slit – 100 μm; objectives – ×50, ×100. We used an onboard He-Ne laser (λ=633 nm, output power 2–20 mW) and Ar+ laser (λ=515 nm and λ= 488 nm, output power 1–100 mW). The duration of signal accumulation varied from 1 to 10 seconds, and the number of measurements in one section of the spectral range was 3-20 times. The spectra were recorded at room temperature +20°C.

The UV Raman spectroscopy studies were carried out at the Keldysh Research Center (Moscow, Russia) using a T64000 spectrometer (Horiba) with the following registration conditions: λ=244 nm; output power: 0.4–1.5 mW; confocal pinhole – 300 μm; grating – 2400 g/mm; slit – 100 μm; objective – ×40 UVB. The signal accumulation period and number of measurements in one spectral range section were 10 sec and 20 times, respectively. The spectra were recorded at room temperature +20°C.

UV Raman spectroscopy studies of natural carbon polyphase aggregate were conducted at the St. Petersburg State University Resource Center «Geomodel» using a LabRam HR spectrometer (Horiba). Registration conditions: λ=325 nm; output power – 5 mW; confocal pinhole – 300 μm; grating – 1800 g/mm; objective – ×40. The signal accumulation period and number of measurements in one spectral range section were 2 sec and 60-80 times, respectively. The spectra were recorded at room temperature +20°C

Raman spectra were curve-fitted by LabSpec 5.36 software using the pseudo-Voigt function, which is a linear combination of a Gaussian curve and a Lorentzian curve, to determine peak positions, their full bandwidth at half maximum (FWHM) and their integral intensity (Table 1). When comparing the band intensity in Raman spectra, the relative peak integral intensities were analyzed upon calculating them as a ratio of one peak area to a total area of all peaks in the spectrum. This value characterizes a peak fraction in Raman spectrum.

The Raman spectra of nanocrystalline graphite and shungite were deconvoluted by the method of Sadezky (2005) and Tan (2004) into the bands and their overtones and combinations – D4, D, D3, G, D2, 2D4, D4 + D, 2D, D3 + D, D + G, 2D2. UV Raman spectra of ultrananocrystalline diamonds were deconvoluted into the diamond line and additional bands at the fixed positions: 1050, 1254, 1590, 1640, 1740 cm^{-1}. In the UV Raman spectra of nanocrystalline diamond, only the line corresponding to T_{2g} mode of diamond is distinguished. The visible Raman spectrum of the polyphase carbon aggregate was deconvoluted similarly into shungite bands, and the UV Raman spectrum was deconvoluted into shungite bands and diamond lines.

To determine the internal nanostructure features of the analyzed carbon substances, TEM and high-resolution TEM (HRTEM) images with corresponding electron diffraction patterns

were obtained (Shumilova et al., 2014, 2016, 2018a, 2019, Ulyashev et al. 2018). The TEM observations were conducted at the Central Facility for Electron Microscopy of RWTH Aachen University (Aachen, Germany) and the Institute of Geology of the FRC Komi SC RAS (Syktyvkar, Russia). The following TEM instruments were used: a high-resolution transmission electron microscope FEI TECNAI F20 equipped with an energy-dispersive X-ray spectrometer (EDX), an energy filter (GATAN imaging filter), a scanning transmission electron microscopy (STEM) unit, and a digital CCD-Camera, operated at 200 kV; and a transmission electron microscope Tesla BS-500, operated at 60 kV. The TEM samples were prepared by the powder method with copper grids with holey carbon films.

Results

The recorded visible Raman spectra of shungite and nanocrystalline graphite samples clearly demonstrate both D and G bands of sp^2 carbon, and there are also D_2, D_3 and D_4 bands, and their overtones and combinations, observed depending on excitation laser radiation: 2450–2500 cm^{-1} (D_4 + D), 2650–2700 cm^{-1} (2D), 2800–2850 cm^{-1} (D_3 + D), 2900–2950 cm^{-1} (D + G) and 3180–3230 cm^{-1} ($2D_2$). The spectra obtained through UV radiation exhibit a distinct difference compared to the visible Raman data, which will be presented below.

Nanocrystalline graphite

Raman spectra of nanocrystalline graphite were recorded in ranges of 100–4000 cm^{-1} for visible excitation and 1000–4000 cm^{-1} for UV. The Raman spectra of graphite with 100-200 nm crystallite sizes (Fig. 2d) with visible excitation contain the bands – D, G, D_2, D_4+D, 2D, D+G, $2D_2$ (Fig. 2a, 2b, Table 1). With decreasing the exciting radiation wavelength from 633 nm to 515 nm, the D-band shifts from 1332 cm^{-1} to 1355 cm^{-1} with $FWHM_D$ widening from 49 to 57 cm^{-1}, and two times decrease in its relative integral intensity from 42 to 21 %. At the same time, the

position of the G-band of graphite shifts slightly from 1581 to 1584 cm^{-1}, where the $FWHM_G$ essentially does not change, and the contribution of the G-band to the total area of the spectrum bands also remains almost the same: 23 % and 25 %.

Under UV excitation the D-band in a Raman spectrum of nanocrystalline graphite is weak, its contribution to the total spectral intensity is only 3 %, and its position shifts from 1332 cm^{-1} (633 nm laser) to 1458 cm^{-1} (244 nm laser) with $FWHM_D$ increasing to 106 cm^{-1}. At the same time, the G-band shifts slightly to 1575 cm^{-1} with $FWHM_G$ decreasing to 19 cm^{-1}, but the relative integral intensity of the G-band increases substantially and reaches 84 %. In the higher spectral range under UV excitation, the combination of D+G bands and the nitrogen line of the ambient air at 2330 cm^{-1} are visible, while other bands are absent in the UV Raman spectra (Fig. 2c).

Shungite

Raman spectra of shungite without microscopically observed crystalline planes (Fig. 3d) were recorded in the spectral range 100–4000 cm^{-1} with visible excitation and 100–2600 cm^{-1} under UV excitation. In visible Raman spectra of shungite (Fig. 3a, 3b) D_4, D, D_3, G, D_2 bands and D_4+D, 2D, D_3+D, D+G, $2D_2$ sub-bands are recognized (Table 1). The position of a G-band depending on the used laser wavelength varies insignificantly – from 1598 to 1595 cm^{-1}, and the $FWHM_G$ slightly increases from 51 to 57 cm^{-1}. The contribution of the G-band to the total integral area of all bands in the spectrum also does not change.

In the meantime, the D-band behaves differently. Using 633 nm and 515 nm lasers we observe a D-band shift from 1329 cm^{-1} to 1349 cm^{-1}, with the corresponding $FWHM_D$ decreasing from 82 to 71 cm^{-1} and significant decrease in the relative integral intensity from 63 to 53 %. Under UV excitation, the D-band becomes unclear in the Raman spectrum of shungite. Its contribution to the total spectrum intensity is 9 %, and the position shifts from 1329 cm^{-1} at a 633 nm laser excitation to 1484 cm^{-1} at a 244 nm laser with the $FWHM_D$ 192 cm^{-1}. In contrast, the

relative G-band integral intensity increases several times (up to 65 %). In addition, under UV excitation, the shungite Raman spectra contain wide bands of a supporting glass substrate – 465, 797, 1064 cm^{-1}, the peaks of atmospheric oxygen – 1553 cm^{-1} and nitrogen – 2328 cm^{-1}; other characteristic bands for the visible excitation listed above for shungite are absent (Fig. 3c).

Ultrahigh-pressure glass-like carbon

Natural ultra-high pressure (UHP) glass-like carbon has been enriched from the Kara impactites, where it is found in association with impact ultrananocrystalline diamond (Shumilova et al. 2019). From HRTEM images, the carbon material appears to have a disordered structure, lacking a truly crystalline arrangement (Fig. 4d). The UHP GLC is characterized by the presence of hollow onion-like structures within an essentially amorphous carbon matrix, indicating the formation under extremely high pressure and temperature conditions (Ulyashev et al., 2018). The structural features differ from the above described shungite that has a low pressure origin.

Raman spectra of natural UHP GLC were recorded in the spectral range 100–4000 cm^{-1} with visible excitation and 500–2600 cm^{-1} under UV excitation. In the visible Raman spectra of UHP GLC (Fig. 4a, 4b), the bands D_4, D, D_3, G and sub-bands 2D, D_3+D, $2D_2$ are recognized (Table 2). The position of a G-band depending on the laser wavelength used varies insignificantly from 1594 to 1600 cm^{-1}, and the corresponding $FWHM_G$ increases from 54 to 75 cm^{-1}. The contribution of G-band to the total integral area of all bands in the spectrum increases from 9-13 % (VIS excitation) to 48% (UV excitation).

At the same time, D-band behaves differently. Using 633 nm and 515 nm lasers, we observe a D-band shift from 1344 cm^{-1} to 1350 cm^{-1}, with a small change of the $FWHM_D$ from 121 to 118 cm^{-1} and the relative integral intensity from 23 to 21 %. Under UV excitation, the D-band shifts to 1411 cm^{-1} with a large increase in $FWHM_D$ up to 329 cm^{-1}. Its contribution to the

236 total spectrum intensity increases significantly from 9 to 52 %. In addition, under UV excitation,
237 the UHP GLC Raman spectra include wide bands of a supporting glass substrate, 789 cm^{-1}, and
238 peak of atmospheric nitrogen, 2333 cm^{-1}. (Fig. 4c).
239
240 **Nanocrystalline diamond**
241 Raman spectra of nanocrystalline diamond with 20-30 nm crystallites (Fig. 5d) under
242 visible laser radiation have a peak of diamond at 1332 cm^{-1} (Fig 5a, 5b) which is overlapped by
243 intense structureless luminescence in the whole range of Raman spectrum registration,
244 significantly complicating the identification of a substance, and in some cases, making it
245 impossible.
246 Under UV laser radiation, the luminescence in the spectrum is absent, thus a distinct Raman
247 bands can be well observed (Table 3). The average value of the diamond T_{2g} mode position is
248 1330 cm^{-1} (Fig. 5c), which is close to that of a bulk high crystalline diamond. The measured
249 $FWHM_{T2g}$ is 18 cm^{-1} depending on the size of the nanocrystallite, which is about 30-50 nm
250 (Shumilova et al. 2018a).
251 **Ultrananocrystalline diamond**
252 Previous studies (Chen et al. 2018; Prawer et al. 2000; Davydov 2003) show that the visible
253 Raman spectroscopy does not provide informative spectra of nanocrystalline and
254 ultrananocrystalline diamonds because of their high luminescence, essentially or completely
255 overlapping the Raman signal. We tested the abilities of UV Raman spectroscopy in the study of
256 ultrananocrystalline diamond samples present as nanocrystalline aggregates with crystallites of 2-
257 5 nm in size (Fig. 6d), separated from the Kara impactites by chemical dissolution (Shumilova et
258 al. 2019). Under visible radiation, the Raman bands of carbon matter are overlapped by extremely
259 high intensity structureless luminescence in the whole range of registration of Raman spectrum

(Fig. 6a, 6b), which leads to the impossibility of phase identification. The luminescence level exceeds the Raman signal by 2-3 orders of magnitude.

Under UV laser excitation, the luminescence is absent in the measured spectral range, and the Raman bands can be clearly observed (Fig. 6c). The UV Raman spectra of ultrananocrystalline diamonds have been deconvoluted into diamond line and additional bands at fixed positions: 1050, 1254, 1590, 1640, 1740 cm^{-1} (Fig. 6 c, Table 3). In the observed spectra, the band at 1321 cm^{-1} ($FWHM_{T2g}$=39 cm^{-1}) corresponds to the T_{2g} diamond mode, shifted from the standard position, presumably due to heating of the nanocrystalline material during the laser excitation (Tan et al. 1998; Zouboulis, Grimsditch 1991). According to Ferrari and Robertson (2004), the observed band at 1050 cm^{-1} (FWHM = 252 cm^{-1}) corresponds to a T-peak, which conforms to the presence of C–C vibrations in a sp^3 carbon state. The observed band at 1254 cm^{-1} (FWHM = 225 cm^{-1}) is present in the Raman spectra of nanodiamonds only by UV excitation resulting from small vibrational domains (Osswald et al. 2009).

By spectra deconvolution, we recognize several additional non-diamond bands corresponding to sp^2 carbon and some radicals. Among them is a well recognized G-band at 1590 cm^{-1} of sp^2 carbon (FWHM=103 cm^{-1}). The band at 1640 cm^{-1} (FWHM=192 cm^{-1}) may belong to the G peak within ta-carbon (Ferrari & Robertson, 2004) or to O–H group vibrations. The band at 1740 cm^{-1} (FWHM=64 cm^{-1}) presumably corresponds to C=O vibrations (Mochalin et al. 2009). The presence of C=O groups in the studied samples was confirmed by IR spectroscopy (Shumilova et al. 2019).

Natural polyphase carbon aggregates

We further studied natural polyphase carbon aggregate (Fig. 7c) separated from the Kara impactites by chemical dissolution. According to HRTEM data (Ulyashev et al. 2018), it contains impact UHP glassy carbon, nanocrystalline diamond and newly formed graphite. The study of

natural polyphase aggregates by visible Raman spectroscopy allowed obtaining informative Raman spectra (Fig. 7a), which turned out to be similar to the spectra of shungite, where the G-band is at 1597 cm^{-1} (FWHM = 58 cm^{-1}), and D-band has a maximum at 1345 cm^{-1} (FWHM = 83 cm^{-1}). Additionally, in the spectrum, D_4- and D_3-bands were registered with positions 1231 cm^{-1} and 1513 cm^{-1}, respectively (Table 4).

Raman spectrum of the carbon polyphase aggregate was recorded under 325 nm ultraviolet laser excitation (Fig. 7b). Deconvolution of the spectrum revealed three bands: the D-band at 1414 cm^{-1} (FWHM = 170 cm^{-1}), the G-band at 1581 cm^{-1} (FWHM = 70 cm^{-1}) and the diamond line at 1325 cm^{-1} (FWHM = 21 cm^{-1}). Thus, the use of ultraviolet laser (325 nm) allowed the detection of diamond in the polyphase carbon aggregate, in addition to shungite, previously discovered by a visible laser (515 nm).

Discussion

D-band nature in sp^2-carbons. It is known that the Raman spectrum of graphite-like carbon substances contains an intense G-band with a maximum at 1570–1610 cm^{-1} (Tan et al. 1999a; Tan et al. 2004; Saito 2010; Ferrari 2007; Tuinstra, Koenig 1970) corresponding to the fundamental Raman mode E_{2g} (Tan et al. 2004), which is responsible for vibrations of carbon atoms inside the graphite layer. In addition, the spectra of disordered graphite or poor-structured sp^2-carbon have an intensive D-band with a band position in the range of 1320–1360 cm^{-1}. While the nature of G-band has been unequivocally established, the nature of D-band remains unclear, thought it has been extensively studied. Initially, the D-band was explained by a breathing mode of sp^2-carbon atoms in carbon rings (Tuinstra, Koenig 1970). The band later received another interpretation, however.

The term “D” - band is coined from the English word, “disordered”. It is important to note that the D-band is absent in the Raman spectrum of an ideal graphite crystal. Its presence and

intensity are associated with a degree of graphite disorder, depending on the size of the graphite crystallite (Reich, Thomsen 2004). It was also noted that the position of D-band depends on the exciting radiation energy. Under exciting by a 515 nm laser, its position is 1350 cm^{-1}; when excited by a 633 nm laser, the D-band is characterized by a shift to the shortwave direction, 1330 cm^{-1} (Reich, Thomsen 2004).

Sood et al. (1998) explained the D-band by double resonance caused by defects in the band structure above slit $\Delta \approx 1$ eV, leading to the dependence of the phonon wave vector q, and hence, the phonon frequency on the incident light energy E_1, as $q \sim (E_1 - \Delta)^{1/2}$. Tan et al. (2004) found discrepancies between the Stokes and anti-Stokes frequencies of the D-band, but they could not provide a reason for this. For the bands of the second-order in graphite, an unusual dependence on the excitation energy was found (Reich, Thomsen 2004). At higher energy laser excitation, the second-order bands are shifted twice faster compared to the first-order bands. At the same time, the effect is not caused by graphite structure defects.

Analyzing the modern theoretical models, Ferrari has shown that the D-band is associated with a longitudinal optical photon (LO phonon) around the K point (Brillouin zone) and is activated by double resonance. Its scattering depends on the excitation energy due to the Kohn anomaly at the K point (Ferrari 2007; Kohn 1959). The Kohn anomaly is described in detail in the semiconductor physics, where the Fermi surface is considered (Kohn 1959; Hasdeo et al 2016).

Pocsik et al. (1998) demonstrated the D-band shift in a Raman spectrum of graphite under excitation by lasers with different energies (λ from 1068 to 300 nm), and it was shown that the position of the D-band (dispersion 40–50 cm^{-1}/eV) at excitation with 244 nm laser is in the range of 1455–1485 cm^{-1}. The shift of the D-band observed in our study with nanostructured sp^2-

carbon leads to an increase in the wave number for the samples of nanocrystalline graphite and shungite at 112–155 cm^{-1}, and the decreases in the band intensity are probably associated with the scattering effect that depends on the excitation energy due to the Kohn anomalies at K point (Kohn 1959).

In studying low-ordered graphite-like substances by UV Raman spectroscopy, we observed that the relative integral intensity of the D–band decreased by 2–14 times and its position shifted up to 112–155 cm^{-1} towards increasing the wavenumber. Correspondingly, the relative intensity of the G-band increased by 2–4 times and had a slight shift of 6–11 cm^{-1} towards the wavenumber decreasing. Thus, a clearly distinguished D-band in the visible-Raman spectra was barely noticeable in UV excitation spectra.

It is clear from the above data that the decrease in the wavelength of the excitation from visible to ultra-violet light results in a substantial "simplification" of the Raman spectrum in the sp^2 carbon crystalline and noncrystalline substances. Under UV excitation, the G-band, as directly related to the vibrations of carbon atoms inside a graphene layer, is demonstrated more clearly, and its relative integrated intensity increases significantly. On the contrary, the D-band in UV Raman spectra has a resonant nature and shifts in sp^2-carbons from 1330 cm^{-1} (633 nm laser) to 1444–1484 cm^{-1} (244 nm laser) and becomes almost invisible in a UV spectrum relative to the G-band. Note that the shift of the D-band position observed under UV radiation cannot be associated with laser heating during the process of Raman scattering excitation, since heating would result in band shifts towards decreasing the wavenumber (Tan et al. 1999a).

Raman features of nanostructured sp^2-carbons. Comparing the spectra of shungite and nanocrystalline graphite under UV excitation, we can draw the following conclusions. At first glance, the UV Raman spectra are similar. If a slight shift in the position of the G-band can be attributed to thermal heating during the registration of Raman spectra, then the FWHM of the G-

band differs significantly; the FWHMs for shungite and nanocrystalline graphite are 39 cm^{-1} and29 cm^{-1}, respectively (Table 2). Thus, the main distinguishing feature of shungite from nanocrystalline graphite is the FWHM of the G-band. For the shungite, we observe a very low D band (1484 cm^{-1}), as occurred in graphite (Ferrari & Robertson, 2001, 2004).

Our studied UHP glass-like carbon samples, which were formed at impact conditions in tight genetic and spatial relation with nano- and ultrananocrystalline diamond, display different UV Raman spectra (Fig. 4c) from those of the above described low pressure shungite. The UHP GLC is characterized by a quite intensive wide Raman band centered at 1411 cm^{-1} that can be assigned to the D-band of sp^2 carbon, which should be absent at UV excitation (Ferrari & Robertson, 2001, 2004). Ferrari and J. Robertson (2001, 2004) showed that the D-peak intensity strongly depends on the order of sp^2 sites and the D-peak could be observed in sp^2-carbons presented with disordered rings structures. Our TEM observation revealed an essentially amorphous structure at the atomic level (Fig. 4d), explaining the relatively high intensity of D-band (Fig. 4c).

Thus, according to Ferrari & Robertson (2001, 2004) and our TEM data of the analyzed carbons, we can conclude that the observed D-band in natural glass-like carbons (low pressure shungite and impact ultrahigh-pressure GLC) is indicative of defect structures with varying degrees of carbon ring disorder.

Raman features of nanostructured sp^3-carbons. Our results demonstrate excellent analytical capabilities for the characterization of ultrananocrystalline diamonds with crystallite sizes of 2–5 nm (Fig. 5, Table 3). The diamond type has been actively studied as one of the most novel types of carbon materials (Chen et al. 2018; Davydov et al. 2004; Davydov et al. 2006; Shenderova, Gruen 2006).

It should be particularly noted that UV excitation for Raman spectra does not significantly change the position of a fundamental sp^3-carbon band compared to the excited spectra by radiation of the visible light, which was previously discussed in detail by Ferrari and Robertson (Ferrari 2007; Ferrari, Robertson 2001, 2004). However, the experimentally measured position of a T_{2g}-mode of diamond essentially depends on the size of the diamond nanocrystallites, with overheating of the ultrananocrystalline diamond. We argue here that to exclude a temperature shift of a T_{2g}-mode of diamond due to laser heating during spectra collection, especially for nanocrystalline samples, the position of the diamond line in the Raman spectrum has to be carefully controlled. For accurate measurements, it is necessary to record Raman spectra at the lowest possible laser power. This provides the possibility of obtaining spectra without a peak shift caused by laser overheating. The decrease in laser power leads to significant increase of exposure time. However, only under these conditions can we be sure that the shift of the diamond line is associated with the structural features of the sample and not with over-heating during the registration of the Raman spectrum.

In this study, we were able to obtain Raman spectra with minimal or no thermal shift of the bands. This was achieved by using a low power of the laser radiation, which helped in maintaining the integrity of the Raman signal decreases. To minimize the impact of noise in the spectra, we increased the exposure time by increasing the number of spectra counts within the shortest possible time, achieving a signal-to-noise ratio of at least 3. This approach can be used for accurate Raman measurements aimed at analyzing some structural features of nanocomposite sp^3-carbons with either visible or UV excitations.

At the same time, we must note that nanodiamonds and diamond-like carbons (DLC) have additional bands in their Raman spectra resulting from a large number of sp^2 sets at their edge boundaries and amorphous carbon matrix of DLC and specific bands corresponding to the

This is the peer-reviewed, final accepted version for American Mineralogist, published by the Mineralogical Society of America.
The published version is subject to change. Cite as Authors (Year) Title. American Mineralogist, in press.
DOI: https://doi.org/10.2138/am-2022-8912. http://www.minsocam.org/

amorphous state of sp^3 sets (Ferrari & Robertson, 2004). The additional bands are presented with D and G bands of sp^2 carbon, similar to that described above for sp^2 monophase substances.

From the measured UV Raman spectra, the ultrananocrystalline diamond is presented not only with tiny-sized diamond crystallites but also with tetrahedral amorphous diamond-like carbon (ta-carbon),which has a high content of sp^3 carbon sites characterized by T and G bands of DLC, at 1050 cm^{-1} (FWHM = 252 cm^{-1}) and 1640 cm^{-1} (FWHM=192 cm^{-1}), respectively (Table 3). It is especially important that the mentioned T band can be visible only under UV excitation. According to simulations, it corresponds to C–C sp^3 vibration density of states of ta-carbon (Ferrari & Robertson, 2004). From the data of ultrananocrystalline diamond (Ferrari and Robertson 2004), it is expected that the DLC matrix is presented with a high content of sp^3 carbon (about 85 %). For a more certain interpretation of the additional bands, additional TEM studies with electron energy loss spectroscopy are needed.

Aggregates of nanostructured sp^2 and sp^3 carbons. Our data clearly demonstrate that UV excitation provides a technical possibility to analyze differently aggregated sp^2 and sp^3 carbons from nanocrystalline tight growths to ultrananocrystalline diamond with the possible presence of diamond-like amorphous tetrahedral sp^3 carbon (Fig. 7). It is also possible to analyze structural features of nanostructural carbons, including C-H and C=O vibrations and other hetero-elemental bonding within carbon substances. The use of UV Raman spectroscopy does not require the preparation of special specimens and can be a convenient and user-friendly method in addition to TEM studies of nanostructured carbons.

Implications

The Raman spectral features of natural low-ordered carbon substances excited by lasers of different wavelengths have been demonstrated. For the first time we have provided a detailed

426 description of the spectroscopic characteristics obtained under UV radiation for natural
427 nanocrystalline graphite, shungite, UHP glass-like carbon, as well as for natural nanocrystalline
428 and ultrananocrystalline diamonds with crystallite sizes of 2-5 nm and polyphase carbon
429 aggregates. The results demonstrate new perspectives for future studies of natural low-ordered
430 sp^2 carbons using Raman spectroscopy with UV excitation.

431 This study has the potential to significantly enhance our understanding of the structural
432 characteristics and polymeric features of low-structured natural carbon matter with varying sp^2-
433 site orders.A significant decrease in intensity and a considerable shift of the D-band in the Raman
434 spectra of low-ordered sp^2-carbon substances using UV excitation allow for the distinction
435 between sp^2 and sp^3 carbons when they coexist in nano- and ultrananocrystalline individual and
436 polyphase samples. The latter is explained by the constancy of sp^3-carbon upon excitation of
437 Raman scattering by both visible and ultraviolet radiations. UV Raman spectroscopy offers
438 convenient and user-friendly features that make it an excellent tool for studying nanostructured
439 carbons. It can effectively analyze the phase composition and ordering characteristics of low-
440 ordered multicomponent natural carbon substances, including sp^3- and sp^2-carbons in polymeric
441 or nanocrystalline substances. Additionally, UV Raman spectroscopy is highly suitable for
442 studying nanocrystalline and ultrananocrystalline diamonds, as well as polyphase tight
443 intergrowths. Its detailed spectroscopic characteristics enable precise characterization and
444 differentiation of different carbon structures, making it a valuable technique for future research in
445 this field.

446 Finally, the use of UV Raman spectroscopy may provide a more accurate understanding of
447 the real phase compositions of nanostructured natural carbons for their potential technological
448 applications.

449

Acknowledgments and funding

The authors are thankful to Valeriy Kazakov for help in UV Raman measurements, Joachim Mayer for help in preliminary TEM studies, Mikhail Filippov for providing samples of shungite and to Sergey Tkachev for valuable comments. The study was carried out with support of the project NIR 122040600009-2.

References cited

Berdnikov, N.V., Shumilova, T.G., Pyachin, S.A., Pugachevsky, M.A., Cherepanov, A.A., Isaenko, S.I. Karpovich, N. F., and Komarova, V. S. (2014) Phase state of the carbonaceous matter in the metalliferous shales of the Russian Far East. Russian Journal of Pacific Geology, 8(4), 268–275.

Beyssac, O., Goffé, B., Chopin, C., and Rouzaud, J.N. (2002) Raman spectra of carbonaceous material in metasediments: a new geothermometer. Journal of Metamorphic Geology, 20(9), 859–871. https://doi.org/ 10.1046/j.1525-1314.2002.00408.x.

Buseck, P.R., Galdobina, L.P., Kovalevski, V.V., Rozhkova, N.N., Valley, J.W., and Zaidenberg, A.Z. (1997) Shungites: the carbon-rich rocks of Karelia. Canadian Mineralogist, 35(6), 1363–1378.

Buseck, P.R., Tsipursky, S.J., and Hettich, R. (1992) Fullerenes from the geological environment. Science, 257, 215–217.

Chen, K., Mei, Y.S., Cui, J.M., Li, X., Jiang, M.Y., Lu, S.H., and Hu, X.J. (2018) Man-made synthesis of ultrafine photoluminescent nanodiamonds containing less than three silicon-vacancy colour centres. Carbon, 139, 982–988. https://doi.org/10.1016/j.carbon.2018.08.013.

Danilova, Yu.V., Isaenko, S.I., and Shumilova, T.G. (2015) Estimation of the conditions of fluid carbonization. Doklady Earth Sciences, 463(2), 787.

Davydov, V.A., Rakhmanina, A.V., Agafonov, V., Narymbetov, B., Boudou, J.P., and Szwarc, H. (2004) Conversion of polycyclic aromatic hydrocarbons to graphite and diamond at high pressures. Carbon, 42, 261–269.

Davydov, V.A., Rakhmanina, A.V., Boudou, J.P., Thorel, A., Allouchi, H., and Agafonov, V. (2006) Nanosized carbon forms in the processes of pressure – temperature-induced transformations of hydrocarbons. Carbon, 44, 2015–2020.

Ferrari, A.C. (2002) Determination of bonding in diamond-like carbon by Raman spectroscopy. Diamond and Related Materials, 11, 1053–1061.

Ferrari, A.C. (2007) Raman spectroscopy of graphene and graphite: Disorder, electron–phonon coupling, doping and nonadiabatic effects. Solid State Communications, 143, 47–57.

Ferrari, A.C., and Robertson, J. (2001) Resonant Raman spectroscopy of disordered, amorphous, and diamondlike carbon. Physical review B, 64, 075414.

Ferrari, A.C., and Robertson, J. (2004) Raman spectroscopy of amorphous, nanostructured, diamond-like carbon, and nanodiamond. Philosophical Transactions of the Royal Society of London A, 362, 2477–2512.

Filik, J., Harvey, J.N., Allan, N.L., and May, P.W. (2006) Raman spectroscopy of nanocrystalline diamond: An ab initio approach. Physical Review B, 74, 035423.

Golubev, Ye.A. (2013) Electrophysical properties and structural features of shungite (natural nanostructured carbon). Physics of the Solid State, 55(5), 1078–1086. https://doi:10.1134/s1063783413050107.

Golubev, Ye.A., Isaenko, S.I., Prikhodko, A.S., Borgardt, N.I., and Suvorova, E.I. (2016) Raman spectroscopic study of natural nanostructured carbon materials: shungite vs. anthraxolite. European Journal of Mineralogy, 28(3), 545–554.

Goryainov, S.V., Likhacheva, A.Y., Rashchenko, S.V., Shubin, A.S., Afanas'ev, V.P., and Pokhilenko, N.P. (2014) Raman identification of lonsdaleite in Popigai impactites. Journal of Raman Spectroscopy, 45, 305–313. https://doi.org/10.1002/jrs.4457.

Gupta, V., Nakajima, T., Ohzawa, Y., and Zemva, B. (2003) A study on the formation mechanism of graphite fluorides by Raman spectroscopy. Journal of Fluorine Chemistry, 120, 143-150. https://doi:10.1016/S0022-1139(02)00323-8.

Hasdeo, E.H., Nugraha, A.R.T., Dresselhaus, M.S., and Saito, R. (2016) Fermi energy dependence of first- and second-order Raman spectra in graphene: Kohn anomaly and quantum interference effect. Physical review B, 94, 075104.

Isaenko, S.I., Shumilova, T.G., and Kazakov, V.A. (2018) Advantages of ultraviolet Raman spectroscopy in the study of nanostructured carbon substances. Bulletin of the Institute of Geology, Komi Scientific Center, Ural Branch of the Russian Academy of Sciences, 12, 46–51. (on Russian) https://doi.org/10.19110/2221-1381-2018-12-46-51.

Khanchuk, A.I., Berdnikov, N.V., Shumilova, T.G., Pyachin, S.A., and Pugachevskii, M.A. (2013) Mineralogical–geochemical characteristics of graphite in carbon-bearing schists of the Russian Far East: New Data. Doklady Earth Sciences, 451(2), 830–833.

Kis, V.K., Shumilova, T., and Masaitis, V. (2016) HRTEM study of Popigai impact diamond: heterogeneous diamond nanostructures in native amorphous carbon matrix. Physics and Chemistry of Minerals, 43(9), 661–670. https://doi.org/10.1007/s00269-016-0825-6.

Kohn, W. (1959) Image of the Fermi surface in the vibration spectrum of a metal. Physical review letters, 2(9), 393–394.

Kovalevski, V.V. (2008) Fullerene-like carbon in nature and perspectives of its use in science-based technologies. Minerals as Advanced Materials, I, 165–168.

Kovalevski, V.V., Buseck, P.R., and Cowley, J.M. (2001) Comparison of carbon in shungite rocks to other natural carbons: an X-ray and TEM study. Carbon, 39, 243–256.

Krishnan, R.S. (1946) Temperature variations of the Raman frequencies in diamond. Proceedings of Indian academy of sciences (mathematical sciences), 24, 45.

Melezhik, V.A., Filippov, M.M., and Romashkin, A.E. (2004) A giant palaeoproterozoic deposit of shungite in NW Russia: genesis and practical applications. Ore Geology Reviews, 24, 135–154.

Merlen, A., Buijnsters, J., and Pardanaud, C. (2017) A guide to and review of the use of multiwavelength Raman spectroscopy for characterizing defective aromatic carbon solids: from graphene to amorphous carbons. Coatings, 7(10). https://doi.org/10.3390/coatings7100153.

Mermoux, M. (2017) Raman investigations on nanodiamonds. In micro and nano technologies, nanodiamonds. Elsevier, 85–107. https://doi.org/10.1016/B978-0-32-343029-6.00004-0.

Mochalin, V., Osswald, S., and Gogotsi, Y. (2009) Contribution of functional groups to the raman spectrum of nanodiamond powders. Chemistry of Materials, 21, 273–279.

Osipov, V.Yu., Panich, A.M., and Baranov, A.V. (2018) Comment on “Carbon structure in nanodiamonds elucidated from Raman spectroscopy” by V.I. Korepanov et al. Carbon, 127, 193–194. https://doi.org/10.1016/j.carbon.2017.11.004.

Osswald, S., Mochalin, V.N., Havel, M., Yushin, G., and Gogotsi, Y. (2009) Phonon confinement effects in the raman spectrum of nanodiamond. Physical review B, 80, 075419. https://doi.org/10.1103/PhysRevB.80.075419.

Piscanec, S., Lazzeri, M., Mauri, F., Ferrari, A.C., and Robertson, J. (2004) Kohn anomalies and electron-phonon interactions in graphite. Physical review letters, 93(18), 185503. https://doi:10.1103/PhysRevLett.93.185503.

Plyusnina, L.P., Shumilova, T.G., Isaenko, S.I., Likhoidov, G.G., and Ruslan, A.V. (2013) Graphite of the Turgenevskoe and Tamginskoe deposits of the Lesozavodsk area in the Primor'e region. Russian Journal of Pacific Geology, 7(4), 288.

Pocsik, I., Hundhausen, M., Koos, M., and Ley, L.J., 1998. Origin of the D-peak in the raman spectrum of microcrystalline graphite. Journal of Non-Crystalline Solids, 1083, 227–230. https://doi:10.1016/S0022-3093(98)00349-4.

Prawer, S., Nugent, K.W., Jamieson, D.N., Orwa, J.O., Bursill, L.A., and Peng, J.L. (2000) The Raman spectrum of nanocrystalline diamond. Chemical Physics Letters, 332, 93–97. https://doi.org/10.1016/S0009-2614(00)01236-7.

Reich, S., and Thomsen, C. (2004) Raman spectroscopy of graphite. Philosophical transactions of the Royal society A, 362, 2271–2288.

Sadezky, A., Muckenhuber, H., Grothe, H., Niessner, R., and Poschl, U. (2005) Raman microspectroscopy of soot and related carbonaceous materials: spectral analysis and structural information. Carbon, 43, 1731–1742.

Saito, R., Furukawa, M., Dresselhaus, G., and Dresselhaus, M.S. (2010) Raman spectra of graphene ribbons. Journal of physics: condensed matter, 22, 334203. https://doi.org/10.1088/0953-8984/22/33/334203.

Shenderova, O.A., and Gruen, D.M. (2006) Ultrananocrystalline diamond: synthesis, properties, and applications, 416 p. William Andrew Publishing: Norwich, USA.

564 Shumilova, T, Kis, V., Masaitis, V., Isaenko, S., and Makeev, B. (2014) Onion-like
565 carbon in impact diamonds from Popigai astrobleme. European Journal of Mineralogy, 26,
566 267–277.

567 Shumilova, T.G, Isaenko, S.I., and Divaev, F.K. (2013) Mineralogical features of
568 diamond, amorphous diamond-like carbon and graphite from Chagatay carbonatites
569 (Uzbekistan). Mineralogical Journal (Ukraine), 35(2), 81–89.

570 Shumilova, T.G., Isaenko, S.I., Ulyashev, V.V., Kazakov, V.A., and Makeev, B.A.
571 (2018a) Aftercoal diamonds: enigmatic type of impact diamonds. European Journal of
572 Mineralogy, 30, 61–76. https://doi.org/10.1127/ejm/2018/0030-2715.

573 Shumilova, T.G., Lutoev, V.P., Isaenko, S.I., Kovalchuk, N.S., Makeev, B.A., Lysiuk,
574 A.Yu., Zubov, A.A., and Ernstson, K. (2018b) Spectroscopic features of ultrahigh-pressure
575 impact glasses of the Kara astrobleme. Scientific Reports, 8(1).
576 https://doi.org/10.1038/s41598-018-25037-z.

577 Shumilova, T.G., Shevchuk, S.S., and Isaenko, S.I. (2016) Metal concentrations and
578 carbonaceous matter in the black shale type rocks of the Urals. Doklady Earth Sciences,
579 469(1), 695–698.

580 Shumilova, T.G., Ulyashev, V.V., Kazakov, V.A., Isaenko, S.I., Svetov, S.A.,
581 Chazhengina, S.Yu., and Kovalchuk, N.S. (2019) Karite – diamond fossil: a new type of
582 natural diamond. Geoscience Frontiers, 11(4), 1163–1174.
583 https://doi.org/10.1016/j.gsf.2019.09.011.

584 Sood, K., Gupta, R., Munro, C.H., and Asher, S.A. (1998) Proceedings of the XVI
585 international conference on Raman spectroscopy, edited by A. M. Heyns. Wiley–VCH, Berlin
586 62.

Sun, Z., Shi, J.R., Tay, B.K., and Lau, S.P. (2000) UV Raman characteristics of nanocrystalline diamond films with different grain size. Diamond and Related Materials, 9(12), 1979–1983. https://doi.org/10.1016/S0925-9635(00)00349-6.

Sychov, M.M., Mjakin, S.V., Ogurtsov, K.A., Rozhkova, N.N., Matveychikova, P.V., Belyaev, V.V., Vysikailo, F.I., and Nakanishi, Y. (2016) Effect of shungite nanocarbon deposition on the luminescent properties of ZnS:Cu particles. Recent global research and education: technological challenges. Proceedings of the 15th international conference on global research and education inter-academia, 19–23. https://doi.org/10.1007/978-3-319-46490-9_3.

Tan, P., Deng, Y., Zhao, Q., and Cheng, W. (1999a) The intrinsic temperature effect of the Raman spectra of graphite. Applied Physics Letters, 74, 1818–1820.

Tan, P., Dimovski, S., and Gogotsi, Y. (2004) Raman scattering of non-planar graphite: arched edges, polyhedral crystals, arched edges, polyhedral crystals. Philosophical Transactions of the Royal Society A, 362, 2289–2310.

Tan, P.H., Deng, Y.M., and Zhao, Q. (1998) Temperature-dependent Raman spectra and anomalous Raman phenomenon of highly oriented pyrolytic graphite. Physical Review B. 5, 5435–5439.

Tan, P.H., Tang, Y., and Deng, Y.M. (1999b) Resonantly enhanced Raman scattering and high-order Raman spectra of single-walled carbon nanotubes. Applied Physics Letters, 75(11), 1524–1526. https://doi.org/10.1063/1.124743.

Tuinstra, F., and Koenig, J.L. (1970) Raman Spectrum of Graphite. Journal of Chemical Physics, 53, 1126–1130.

Ulyashev, V.V., Shumilova, T.G., Kulnitsky, B.A., Perezhogin, I.A., and Blank, V.D. (2018) Nanostructural features of carbon polyphase aggregates in apocoal products of impact

metamorphism. Bulletin of the Institute of Geology, Komi Scientific Center, Ural Branch of the Russian Academy of Sciences, 8, 26–33. (on Russian) https://doi.org/10.19110/2221-1381-2018-8-26-33.

Wang, L., Liu, B., Li, H., Yang, W., Ding, Y., Sinogeikin, S.V., Meng, Y., Liu, Z., Zeng, X.C., and Mao, W.L. (2012) Long-range ordered carbon clusters: a crystalline material with amorphous building blocks. Science, 337, 825–828.

Wopenka, B., and Pasteris, J.D. (1993) Structural characterization of kerogens to granulite-facies graphite: applicability of Raman microprobe spectroscopy. The American Mineralogist, 78(5/6), 533–557.

Yasumaru, N., Miyazaki, K., and Kiuchi, J. (2004) Glassy carbon layer formed in diamond-like carbon films with femtosecond laser pulses. Applied Physics A, 79(3), 425. https://doi.org/10.1007/s00339-004-2746-3.

Zouboulis, E.S., and Grimsditch, M. (1991) Raman scattering in diamond up to 1900 K. Physical Review B, 43, 12490. https://doi.org/10.1103/PhysRevB.43.12490.

Figure 1. Geographic position of the studied objects. (1) The Nerkayu complex (N65° E61°with nanocrystalline graphite. (2) Shun'ga deposit (N62° E35°) with shungite carbon; (3) Kara astrobleme (N69° E64°) with impact nano- and ultrananocrystalline diamond, impact natural UHP glass-like carbon.

Figure 2. Nanocrystalline graphite. Raman spectra at different wavelengths excitation (**a**) 633 nm, (**b**) 515 nm, and (**c**) 244 nm. Additional line detected by UV laser radiation is N2-2330 cm^{-1} (room nitrogen); (**d**) magnified range 1000–2000 cm^{-1} of spectrum c; (**e**) TEM image in bright field mode (BF) with corresponding electron diffraction pattern (ED).

Figure 3. Shungite. Raman spectra at different laser wavelengths excitation (**a**) 633 nm, (**b**) 515 nm, (**c**) 244 nm. Additional lines detected by UV laser radiation include SiO_2 glass: 465 cm^{-1}, 797 cm^{-1}, 1064 cm^{-1}; O2-1553cm^{-1}; N2-2328 cm^{-1}.**{{auth: ok?}}** (**d**) TEM image in BF mode with corresponding ED pattern.

This is the peer-reviewed, final accepted version for American Mineralogist, published by the Mineralogical Society of America.
The published version is subject to change. Cite as Authors (Year) Title. American Mineralogist, in press.
DOI: https://doi.org/10.2138/am-2022-8912. http://www.minsocam.org/

Figure 4. Natural carbon glass-like carbon: Raman spectra at different laser wavelengths excitation: (**a**) 633 nm, (**b**) 515 nm, (**c**) 244 nm. Additional lines detected by UV laser radiation in SiO_2 glass: 797, N2-2333 cm^{-1}. (**d**) TEM image in BF mode with corresponding ED pattern (the TEM image is used from (Ulyashev et al. 2018) by permission of the editorial board of Vestnik of Geosciences).

Figure 5. Natural nanocrystalline diamond. Raman spectra at different laser wavelengths excitation (**a**) 633 nm, (**b**) 515 nm, (**c**) 244 nm. (**d**) TEM image in BF mode with corresponding ED pattern.

Figure 6. Natural ultrananocrystalline diamond. Raman spectra at different laser wavelengths excitation: (**a**) 633 nm, (**b**) 515 nm, (**c**) 244 nm. (**d**) TEM image in BF mode with corresponding ED pattern.

Figure 7. Natural carbon polyphase aggregate of ultrananocrystalline diamond (UNCD) and UHP glass-like carbon (GLC). Raman spectra from the aggregate at different laser wavelengths excitation (**a**) 515 nm; (**b**) 325 nm. (**c**) TEM image in BF mode (the TEM image is used from (Ulyashev et al. 2018) by permission of the editorial board of Vestnik of Geosciences).

Table 1. Raman spectra components of nanostructured sp^2 carbon substances

Nanocrystalline graphite									
Laser wavelength	633 nm			515 nm			244 nm		
Band	P	FWHM	A (%)	P	FWHM	A (%)	P	FWHM	A (%)
D	1332	49	42	1355	57	21	1458	106	3
G	1581	24	23	1584	26	25	1575	29	85
D_2	1617	23	4	1622	32	5			
D_4+D	2459	154	8	2454	213	9			
2D	2667	88	15	2710	93	24			
D+G	2921	130	4	2946	214	14	3125	146	12
$2D_2$	3242	300	5	3249	22	2			
Shungite									
Laser wavelength	633 nm			515 nm			244 nm		
Band	P	FWHM	A (%)	P	FWHM	A (%)	P	FWHM	A (%)
D_4	1171	85	4	1172	126	3			
D	1329	82	63	1349	71	53	1484	192	12
D_3	1549	131	6	1532	105	7			
G	1598	51	17	1595	57	18	1587	39	88
D_2	1622	21	1	1618	14	0			
D_4+D	2482	150	1	2502	138	1			
2D	2643	191	3	2684	159	9			
D_3+D	2807	100	0	2819	114	1			
D+G	2913	146	5	2937	126	6			
$2D_2$	3183	102	1	3190	109	1			

Notes: P = band position (cm^{-1}), FWHM = full bandwidth at half maximum (cm^{-1}), A (%) = relative integral intensity of the band (the ratio of the band area to the total area of the bands of

This is the peer-reviewed, final accepted version for American Mineralogist, published by the Mineralogical Society of America.
The published version is subject to change. Cite as Authors (Year) Title. American Mineralogist, in press.
DOI: https://doi.org/10.2138/am-2022-8912. http://www.minsocam.org/

665 the spectrum), laser wavelength = the wavelength of the exciting radiation.
666
667 Table 2. Raman spectra components of ultrahigh-pressure glass-like carbon
668

Ultrahigh-pressure glass-like carbon									
Laser wavelength	633 nm			515 nm			244 nm		
Band	P	FWHM	A (%)	P	FWHM	A (%)	P	FWHM	A (%)
D_4	1243	167	19	1277	194	9			
D	1344	121	23	1350	118	21	1411	329	52
D_3	1531	253	34	1523	279	28			
G	1598	55	9	1600	54	13	1594	75	48
2D	2629	378	9	2662	316	12			
D_3+D	2894	300	6	2919	312	16			
$2D_2$	3181	87	0	3192	102	2			

669 *Notes:* P = band position (cm^{-1}), FWHM = full bandwidth at half maximum (cm^{-1}), A (%) =
670 relative integral intensity of the band (the ratio of the band area to the total area of the bands of
671 the spectrum), laser wavelength = the wavelength of the exciting radiation.
672
673
674 **Table 3.** Raman spectra components of nanostructured diamond under UV excitation (244 nm laser)

Nanocrystalline diamond (sp^3-carbon) (8 samples)			
Crystallite size (nm)	Band position range (average), cm^{-1}	FWHM range (average), cm^{-1}	Band interpretation
30-50	1329–1332 (1330)	12–27 (18)	T_{2g}-diamond
Ultrananocrystalline diamond (mixture of sp^3- and sp^2-carbons) (6 samples)			
Crystallite size (nm)	Band position range (average), cm^{-1}	FWHM range (average), cm^{-1}	Band interpretation
2-5	1318–1322 (1321)	41–54 (47)	T_{2g}-diamond Raman mode
	1050	227–287 (252)	T-peak (C–C vibrations in a sp^3 carbon, sp^3 vibration density of states of ta-carbon)
	1254	217–237 (225)	Nanodiamond (small vibrational domains)
	1590	87–117 (103)	G-band of sp^2 carbon
	1640	169–212 (192)	G-band in DLC (ta-carbon)
	1740	45–87 (64)	C=O vibrations

675 *Notes:* n = number of studied samples, FWHM = full bandwidth at half maximum (cm^{-1})
676

677 **Table 4.** Raman spectra components of polyphase carbon aggregate under visible and UV
678 excitation

Laser wavelength	Band position (cm^{-1})	FWHM (cm^{-1})	A (%)	Band interpretation
325 nm	1325	21	8	T_{2g}-diamond (sp^3 carbon)
	1415	137	38	D-band of sp^2 carbon
	1583	59	54	G-band of sp^2 carbon
514 nm	1231	217	15	D_4-band of sp^2 carbon
	1345	83	39	D-band of sp^2 carbon
	1513	219	27	D_3-band of sp^2 carbon
	1597	58	19	G-band of sp^2 carbon

679
680 *Notes:* FWHM = full bandwidth at half maximum (cm^{-1}), A (%) = relative integral intensity of
681 the band (the ratio of the band area to the total area of the bands of the spectrum), laser
682 wavelength = the wavelength of the exciting radiation.
683

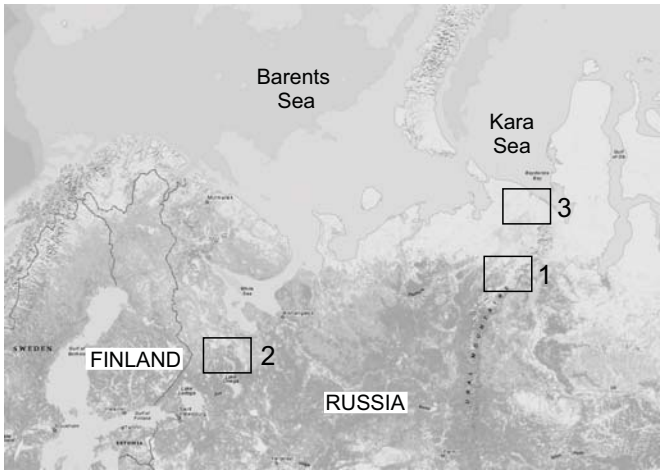

This is the peer-reviewed, final accepted version for American Mineralogist, published by the Mineralogical Society of America.
The published version is subject to change. Cite as Authors (Year) Title. American Mineralogist, in press.
DOI: https://doi.org/10.2138/am-2022-8912. http://www.minsocam.org/

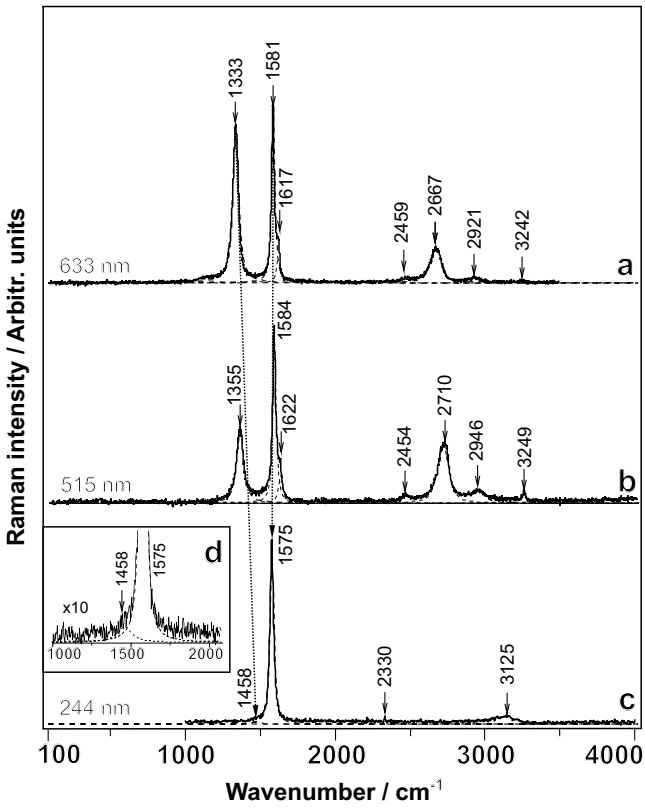

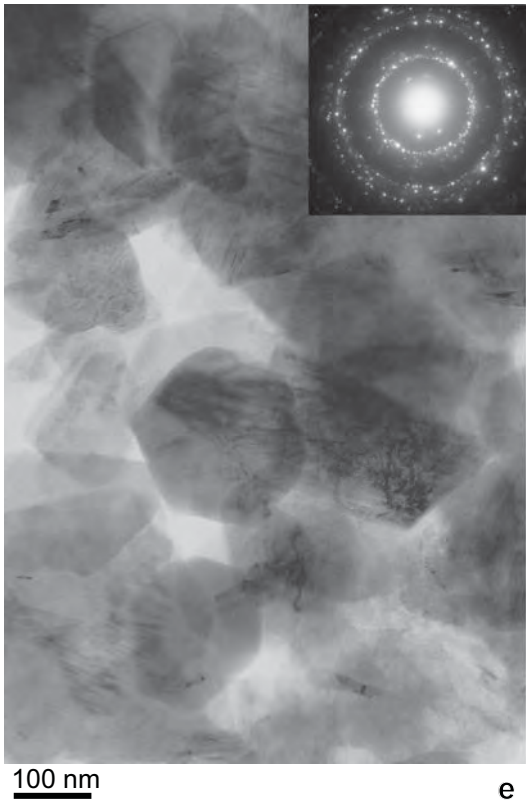

This is the peer-reviewed, final accepted version for American Mineralogist, published by the Mineralogical Society of America.
The published version is subject to change. Cite as Authors (Year) Title. American Mineralogist, in press.
DOI: https://doi.org/10.2138/am-2022-8912. http://www.minsocam.org/

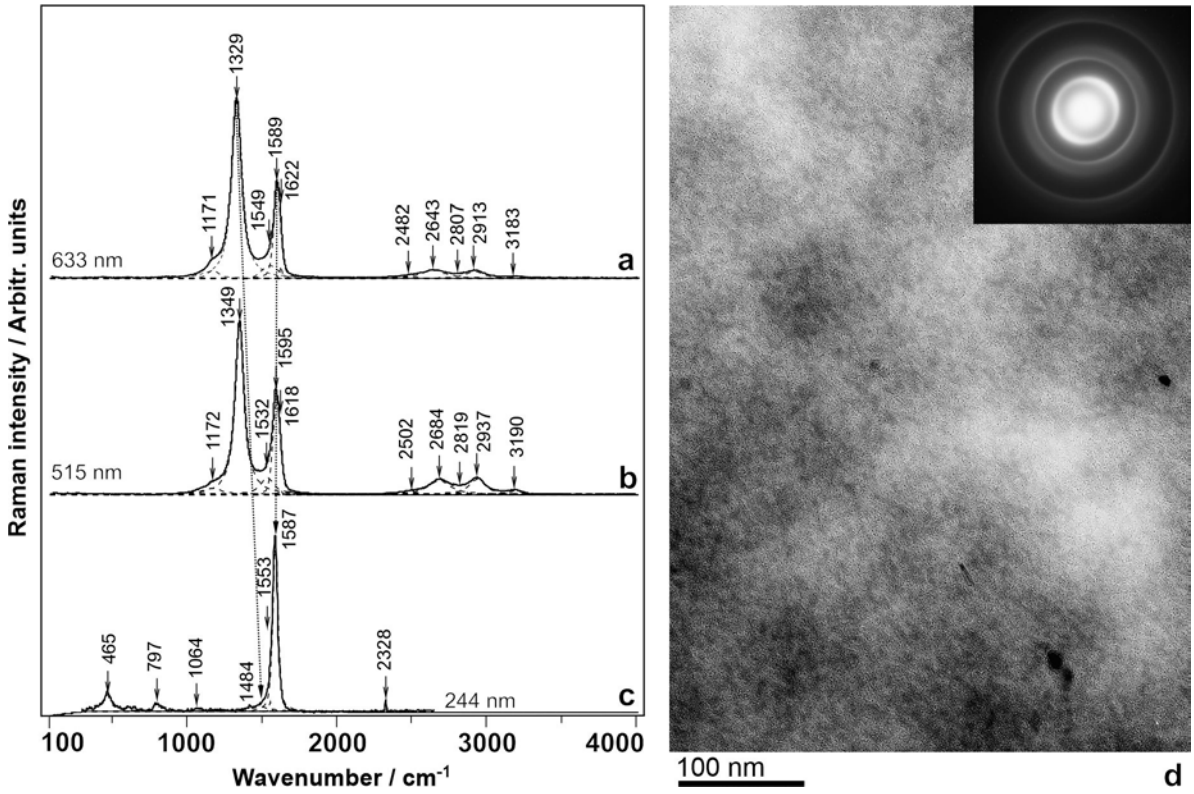

Figure 3.

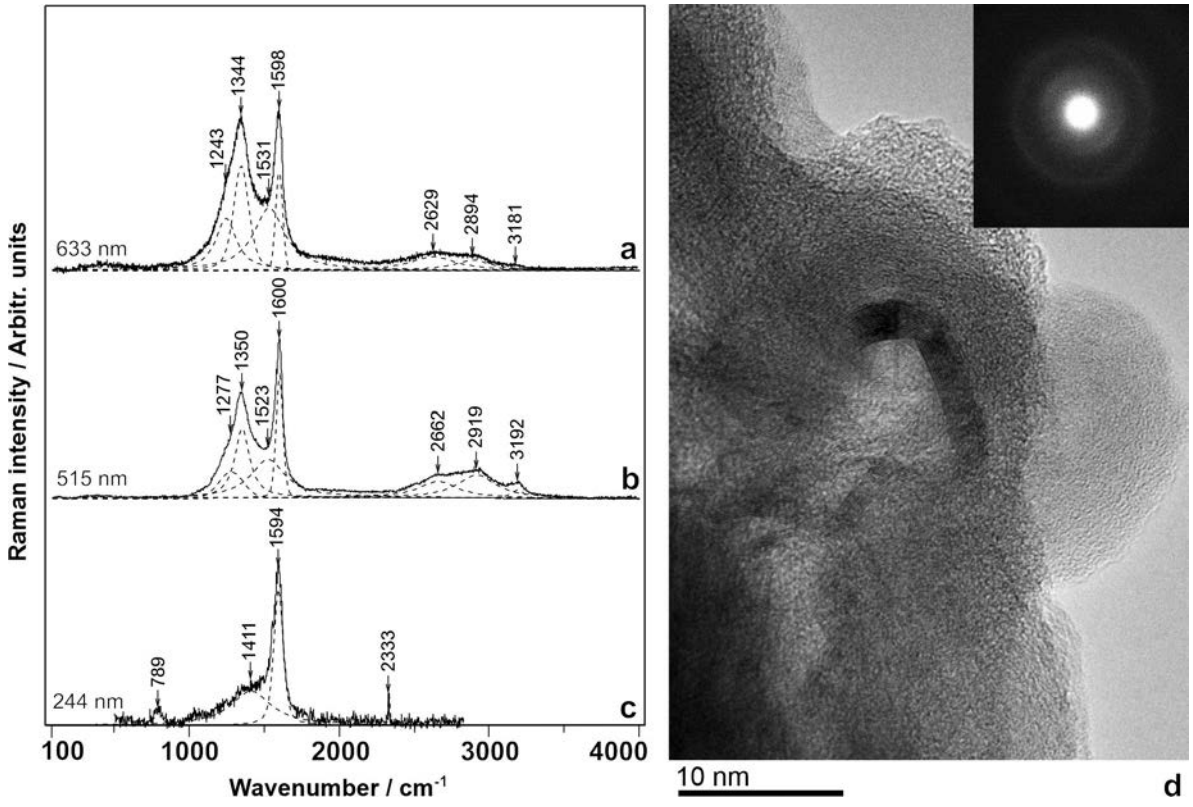

Figure 4.

This is the peer-reviewed, final accepted version for American Mineralogist, published by the Mineralogical Society of America.
The published version is subject to change. Cite as Authors (Year) Title. American Mineralogist, in press.
DOI: https://doi.org/10.2138/am-2022-8912. http://www.minsocam.org/

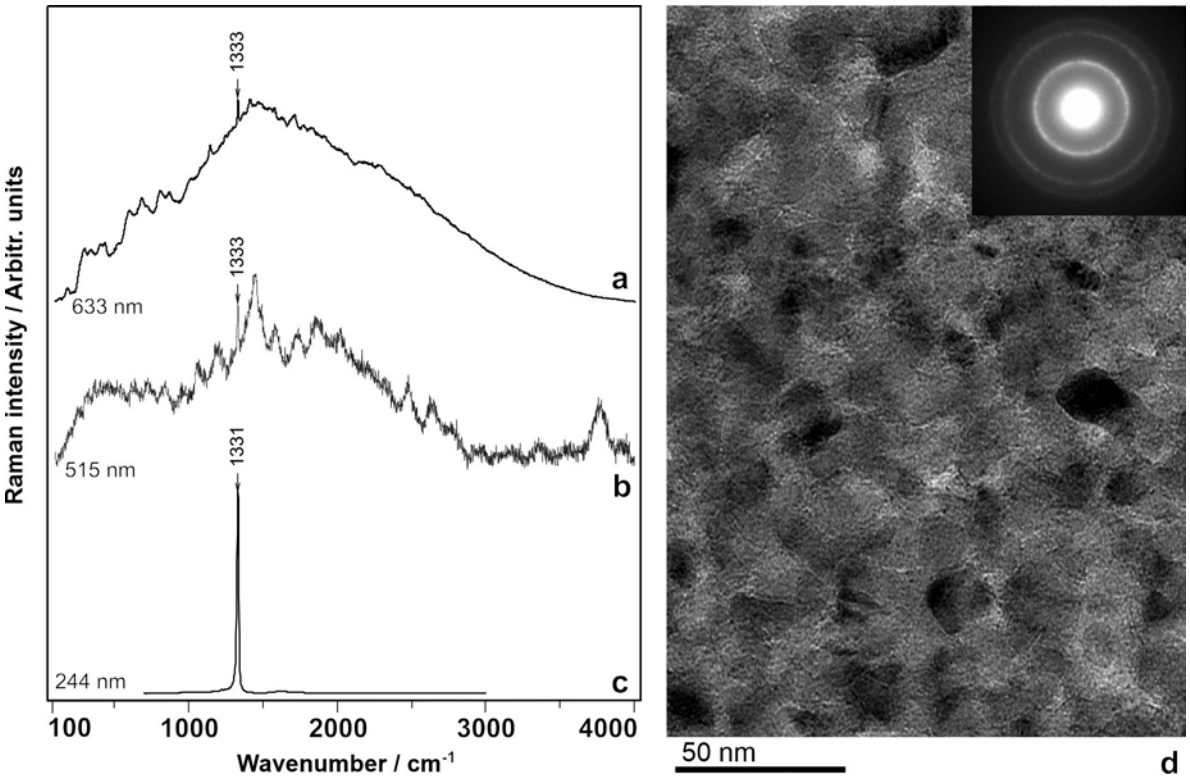

Figure 5.

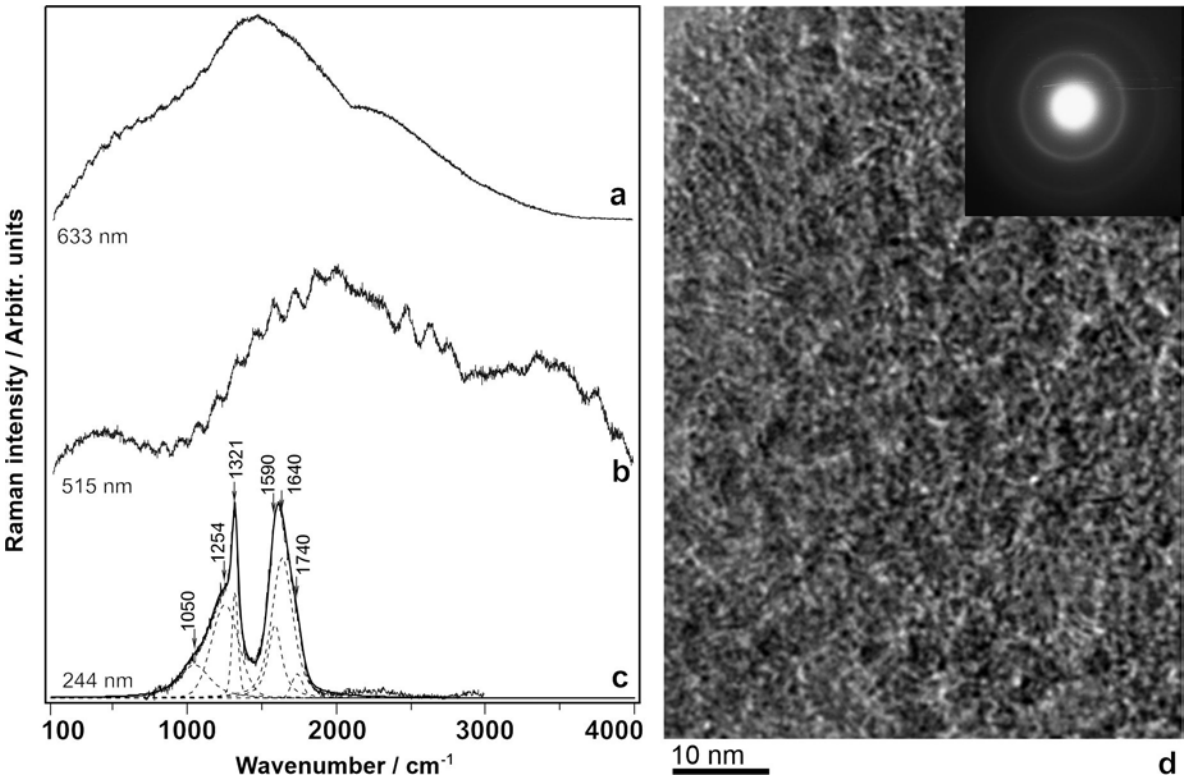

Figure 6.

This is the peer-reviewed, final accepted version for American Mineralogist, published by the Mineralogical Society of America.
The published version is subject to change. Cite as Authors (Year) Title. American Mineralogist, in press.
DOI: https://doi.org/10.2138/am-2022-8912. http://www.minsocam.org/

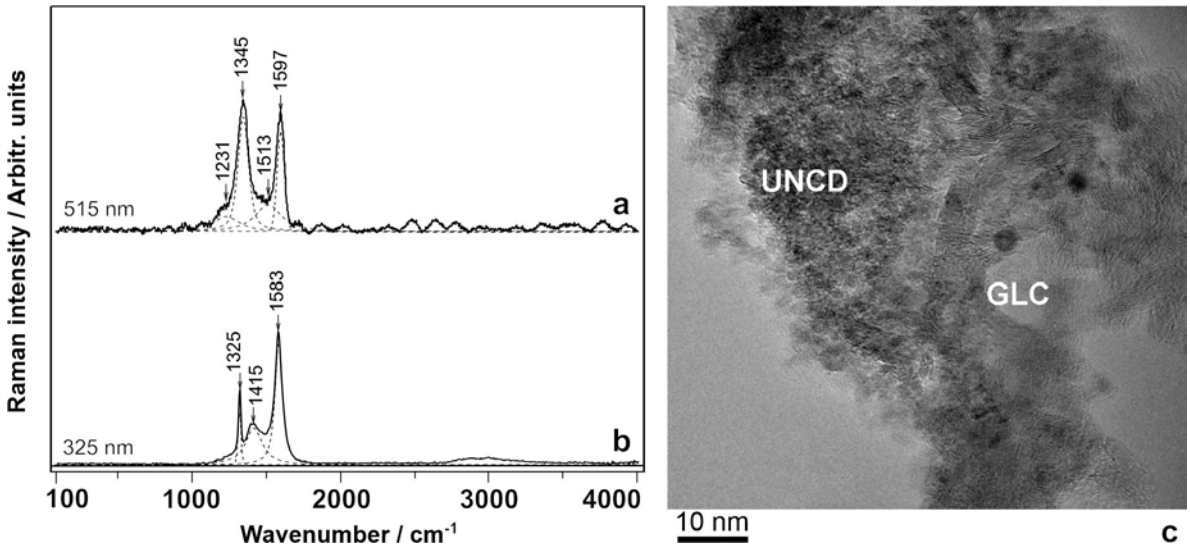

Figure 7.